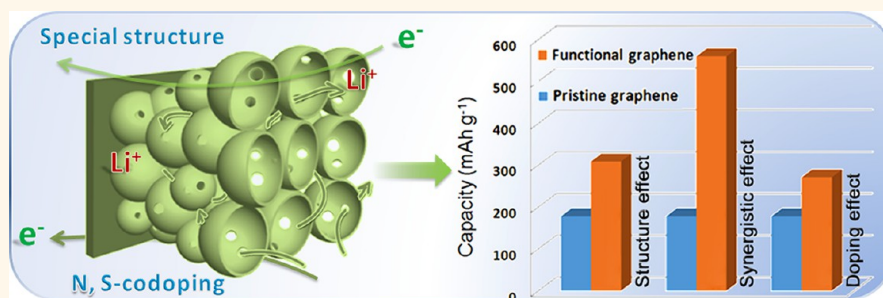


# *In Situ* Fabrication of Porous Graphene Electrodes for High-Performance Energy Storage

Zhong-Li Wang,<sup>†</sup> Dan Xu,<sup>†</sup> Heng-Guo Wang,<sup>†</sup> Zhong Wu,<sup>†,‡</sup> and Xin-Bo Zhang<sup>†,\*</sup>

<sup>†</sup>State Key Laboratory of Rare Earth Resource Utilization, Changchun Institute of Applied Chemistry, Chinese Academy of Sciences, Changchun 130022, People's Republic of China and <sup>‡</sup>University of Chinese Academy of Sciences, Beijing 100049, People's Republic of China

## ABSTRACT



In the development of energy-storage devices, simultaneously achieving high power and large energy capacity at fast rate is still a great challenge. In this paper, the synergistic effect of structure and doping in the graphene is demonstrated for high-performance lithium storage with ultrafast and long-cycling capabilities. By an *in situ* constructing strategy, hierarchically porous structure, highly conductive network, and heteroatom doping are ideally combined in one graphene electrode. Compared to pristine graphene, it is found that the degree of improvement with both structure and doping effects is much larger than the sum of that with only structure effect or doping effect. Benefitting from the synergistic effect of structure and doping, the novel electrodes can deliver a high-power density of 116 kW kg<sup>-1</sup> while the energy density remains as high as 322 Wh kg<sup>-1</sup> at 80 A g<sup>-1</sup> (only 10 s to full charge), which provides an electrochemical storage level with the power density of a supercapacitor and the energy density of a battery, bridging the gap between them. Furthermore, the optimized electrodes exhibit long-cycling capability with nearly no capacity loss for 3000 cycles and wide temperature features with high capacities ranging from -20 to 55 °C.

**KEYWORDS:** energy storage · high power · *in situ* synthesis · synergistic effect · graphene

High-energy and power density energy-storage devices are urgently demanded to meet challenges of the ever-increasing development of large-scale electric energy storage for renewable energy and sustainable road transport.<sup>1–8</sup> Among the electrochemical energy-storage devices, supercapacitors can deliver high power but suffer from low-energy density.<sup>9,10</sup> On the contrary, lithium ion batteries (LIBs) hold high-energy density, but for use as a versatile power source, the power density still needs to be significantly improved.<sup>11–13</sup> In achieving a high-power density of LIBs, many strategies, such as downsizing the electrode materials to nanoparticles (NPs), coating, or mixing with more conductive

materials, and/or doping of electrode materials with foreign atoms have been developed. Although charge and discharge rates are improved, these methods suffer from more or less severe drawbacks such as poor cycling stability (intrinsic agglomeration of small NPs) and requirement of a high percentage of conducting carbon black.<sup>8,11,14</sup> Therefore, it is still a great challenge to significantly enhance both the cyclability and rate capability of LIBs.

Graphene, a one-atom-thick two-dimensional carbon material, is an ideal candidate as a high-power and high-energy anode material for LIBs due to its intrinsically superior electrical conductivity, excellent mechanical flexibility, remarkable thermal

\* Address correspondence to  
xbzhang@ciac.jl.cn.

Received for review December 12, 2012  
and accepted February 5, 2013.

Published online February 05, 2013  
10.1021/nn3057388

© 2013 American Chemical Society

conductivity, and high surface area.<sup>15–22</sup> To turn the alluring promise into reality, many efforts have been made to develop various kinds of graphene-based anode materials, including pure graphene sheets reduced by different methods,<sup>23–27</sup> porous graphene,<sup>28,29</sup> flexible holey graphene paper,<sup>30,31</sup> and heteroatom doping graphene,<sup>32</sup> and high reversible capacity up to 1264 mAh g<sup>-1</sup> at a low rate (50–100 mA g<sup>-1</sup>) has been achieved.<sup>27</sup> However, the rate capability of these materials for high-power applications is still far from satisfying. For example, even a moderate degree of high rate capability still severely depends on addition of a large amount of carbon black NPs.<sup>32</sup> Compared to the numerous reports exploring the intrinsic properties of graphene itself, there is few reports on the rational design and optimization of the graphene electrode structure, which is believed to be essential to further boost the graphene performance in LIBs.<sup>33–40</sup> For example, graphene electrodes prepared by the conventional method with binder suffer from severe graphene aggregation which would inevitably hinder inferior ionic accessibility. What's worse, the randomly and loosely stacked graphene sheets have large interface resistance, which would impede high-rate electron conductivity, especially when insulated binder is added.<sup>32</sup> Consequently, the inefficient ionic and electronic transport in traditional graphene electrodes has led to poor rate capabilities and serious capacity fading on cycling. On the other hand, the latest theoretical research shows that lithium ions can hardly stabilize and diffuse in the graphene without defects. It has been demonstrated that heteroatom doping can introduce much defects in the basal plane of graphene, which increases the lithium ions diffusion and active sites.<sup>41–45</sup> Therefore, design and optimization of structure and doping of the graphene electrode to achieve supercapacitor-like rate capabilities while maintaining battery-like storage capacities are highly desirable yet still very challenging.

Herein, we first demonstrate the synergistic effect of structure and doping in the graphene by designing and fabricating a novel type of doped hierarchically porous graphene (DHPG) electrode through a facile *in situ* constructing strategy in nickel foam using graphene oxide (GO), sulfonated polystyrene (S-PS) spheres, and poly(vinyl pyrrolidone) (PVP) as precursors. Interestingly, the GO and S-PS are assembled into three-dimensional (3D) continuous structure with the assistance of the surfactant of PVP in the nickel foam during evaporation of solvent. After calcination in N<sub>2</sub> atmosphere, the removal of the template and surfactant results in an interconnected porous graphene framework. Thanks to the advantageous combination of the macroporous structure of nickel foam, the formed graphene electrodes hold novel hierarchically porous architectures, which could intrinsically optimize ion transport and also provide sufficient contact

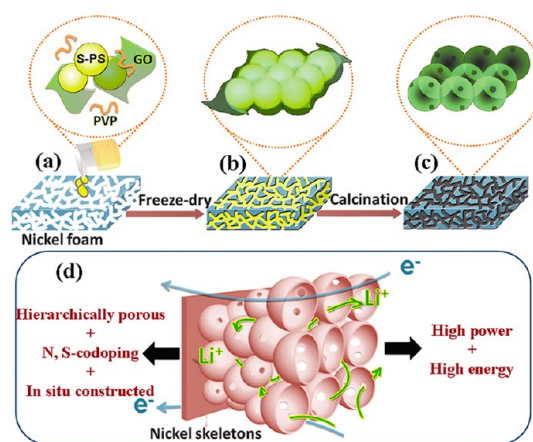


**Figure 1.** Schematic illustration of the synthesis procedures of the DHPG electrodes: (a) impregnating the precursor solution containing GO, PVP, and S-PS into the porous collector of nickel foam; (b) freeze-drying the precursor solution; (c) *in situ* calcining the precursor gel; (d) illustration of the features in the interior structure of DHPG electrodes.

area between the electrode and electrolyte. Furthermore, as porous graphene directly grows on the skeletons of nickel foam without the addition of any binder, high electron conductivity in the electrode assembly can be ensured. It should be noted that, for the first time, nitrogen atoms from PVP and sulfur atoms from S-PS are successfully *in situ* doped into the graphene during pyrolysis of the precursor. Benefitting from the synergistic effect of special structure and heteroatom doping, the as-prepared graphene electrodes exhibit ultrafast, supercapacitor-like discharge and charge rate capabilities while maintaining battery-like storage capacities. Furthermore, the novel electrode is synthesized directly as a whole part and is free of binder and the conventional complex preparation process of anodes, and thus could be of great benefit to large-scale application.

## RESULTS AND DISCUSSION

A schematic illustration of the fabrication process for the DHPG electrode is depicted in Figure 1. The first step of the synthesis process is impregnation of the precursor colloidal solution containing GO, PVP, and S-PS into a freshly washed nickel foam. The SEM and TEM images of GO and S-PS are shown in Figure S1 in the Supporting Information. The sizes of GO are around 1–2  $\mu\text{m}$ , which is smaller than that of S-PS (2.5–3  $\mu\text{m}$ ) and thus can facilitate the assembling of GO on the surface of S-PS. In addition, due to the existence of –COOH in GO and –SO<sub>3</sub>H in S-PS, the precursor solution is weak acid (pH = 1.5), which leads to weakly dissolving of the nickel (Ni) foam. The positively charged Ni<sup>2+</sup> ion would electrostatically interact with the negatively charged GO and S-PS in the Ni foam. Second, the water in the precursor composite is removed using a freeze-drying technology, which ensures the preservation of the uniform dispersion of

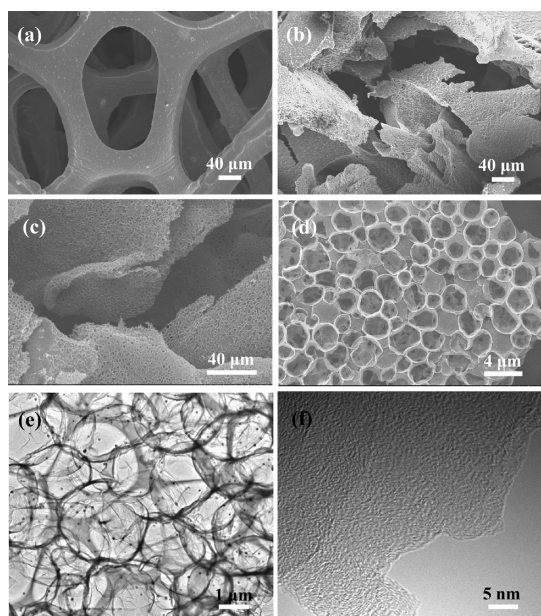


**Figure 2.** SEM images of (a) pristine nickel foam, (b) precursor, (c,d) DHPG electrodes; (e) TEM and (f) HRTEM images of DHPG electrodes.

GO and S-PS in the precursor gel, wherein the PVP interacts with GO and S-PS and thus makes the colloidal system stable. Finally, the DHPG electrodes are obtained by calcining the precursor gel in  $N_2$  atmosphere, where PVP and S-PS are decomposed (Figure S1e), leaving a sphere-like void, and furthermore, part of the nitrogen and sulfur atoms in the PVP and S-PS are *in situ* doped into the graphene at the same time.

The pristine nickel foam with macroporous skeletons is shown in Figure 2a. After *in situ* synthesis of hollow graphene, a visible black coating in the whole nickel foam can be clearly observed (Figure S2). The low-magnification SEM images (Figure 2c and Figure S3) of the DHPG electrodes show that the hollow graphene assemblies exhibit sheet-like morphology. These graphene assembly sheets are loosely packed and aligned roughly perpendicular to the skeleton surface of the Ni foam, which forms a free-standing structure, producing large interconnected tunnels throughout the entire electrode depth. These favorable tunnels would facilitate wetting of the electrolyte and lithium ion transport. From the cross-section images (Figure S4), the sheets grow on the skeletons of nickel foam and adjacent sheets are interconnected with each other. The thickness of the sheets is about 3–10  $\mu m$  with 1–3 layers of S-PS spheres. High-magnification observation (Figure 2d) of the sheets reveals that the sheets consist of hollow graphene spheres with numerous small nanoscale pores between spheres. Some Ni nanoparticles are also observed on the surface of graphene because the dissolved nickel ions are reduced into nickel metal particles by carbon atoms in the graphene gel during

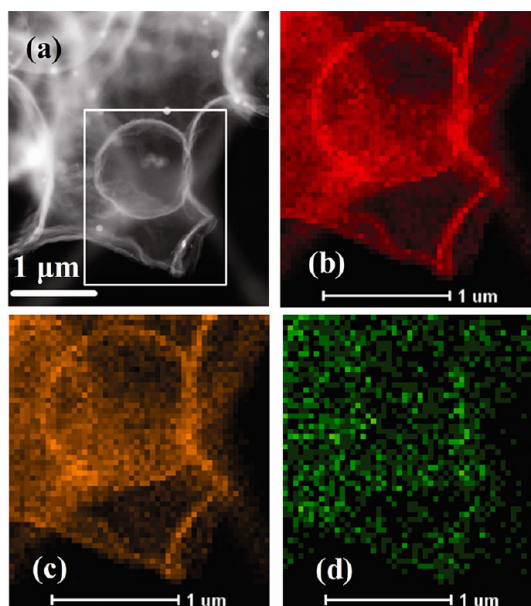


**Figure 3.** (a) STEM image of the N,S-codoped DHPG electrodes; (b) C-, (c) N-, and (d) S-elemental mapping of the square region.

high-temperature treatment (Figure S3e,f). For comparison, no nickel particles are observed if the synthesis is not carried out in nickel foam, while meanwhile, no small pores are observed (Figure S5), indicating that the existence of Ni particles will not only improve the electrical conductivity but also play an important role in creating the pores between spheres. Such interesting phenomenon is further illustrated by two extra experiments (section 5 in Supporting Information), and it can be clearly observed that porous structures are formed during the production of Ni particles (Figure S6). The porous structure of graphene is also confirmed by the TEM image (Figure 2e). In addition, the high-resolution TEM image (Figure 2f and Figure S3d) shows that the thickness of graphene sheets is around 2 nm with 5–6 layers of the single graphene layer. Interestingly, the layer-to-layer distance ( $d$  spacing) is about 0.4 nm, which is larger than that of graphite (0.335 nm). The enlarged  $d$  spacing could facilitate lithium ion diffusion and storage. Furthermore, high-angle annular dark-field scanning transmission electron microscopy (STEM) elemental mapping (Figure 3) reveals that nitrogen and sulfur heteroatoms are uniformly distributed in the graphene sheets. It is also found that the interfaces between graphene spheres grow together (Figure S7), which could alleviate the interface resistance and enable fast electron transport and would benefit the rate capability (*vide infra*). The surface area of the hollow graphene is 70  $m^2 g^{-1}$ , which is three times higher than that of pristine graphene (17  $m^2 g^{-1}$ ), ensuring sufficient contact area between the electrode and electrolyte in the hollow porous structure. On the contrary, when prepared by the conventional method, only seriously aggregated pristine graphene and its

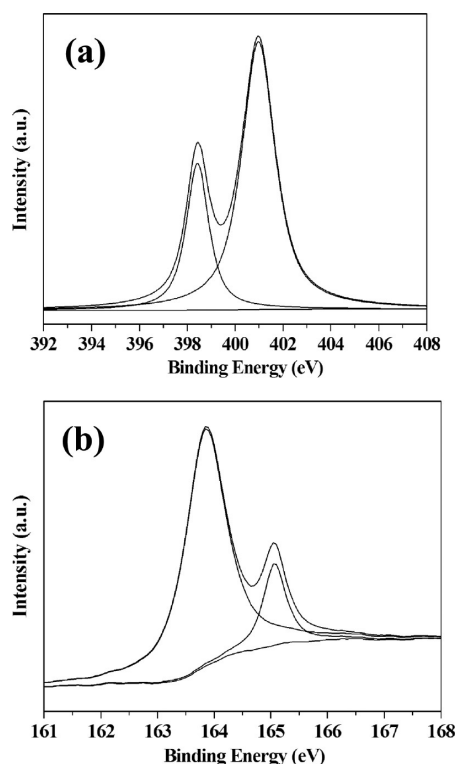


**Figure 4.** (a) N 1s XPS spectrum and (b) S 2p XPS spectrum of doped graphene electrodes.

corresponding electrodes can be obtained (Figure S8). There are two reasons for the relatively low surface area of the DHPG graphene: (1) multiple-layer graphene sheets with enlarged  $d$  spacing are produced during the synthesis process; (2) hollow graphene spheres grow together and form a continuous structure, which leads to partial superposition of graphene sheets. The DHPG is a special 3D graphene structure with the peculiar advantages for Li storage, as illustrated in the following results.

The successful codoping of graphene with N and S atoms is further investigated (elemental compositions and heteroatom bonding configurations) using XPS and Raman spectra. The N 1s and S 2p peaks can be observed in the XPS spectra of DHPG electrodes (Figure S9), further illustrating the coexistence of N and S elements. As shown in Figure 4a, two peaks positioned at 398.4 and 401.0 eV can be identified for the N atoms, corresponding to pyridinic N and quaternary N, respectively,<sup>46</sup> which are formed predominately through substituting a carbon atom by N on edges or defect sites in the plane because such carbon atoms are much more chemically active than those within the plane of perfect graphene. Similarly, two peaks at 163.8 and 165.1 eV are identified in the S 2p XPS spectra, which correspond to the covalent C–S bonds and S–O bonds,<sup>47</sup> respectively (Figure 4b). XPS measurement reveals that the doping level is 4.2% for nitrogen and 0.94% for sulfur. Compared with widely employed surface chemical postmodification method

for graphene doping, for example, ammonia treatment of graphene at high temperature, our work provides a simple *in situ* synthesis route to produce heteroatom-doped graphene. Raman spectra further provide additional proof for the N,S-codoped graphene. With respect to pristine graphene, the increased  $I_D/I_G$  ratio and down-shift of the G band are observed for doped graphene (Figure S10), which is consistent with the previous reports.<sup>48,49</sup>

The electrochemical performance of DHPG electrodes is then investigated as anodes for LIBs. As shown in Figure 5a, the DHPG electrodes show similar cyclic voltammogram curves with pristine graphene electrodes (Figure S11). Two reduction peaks in the potential range of 1.0–1.5 and 0.3–0.9 V are clearly observed in the first cycle. The peak at 1.0–1.5 V is attributed to the reaction of lithium with functional groups at the graphene surface, which has been well-studied in carbonaceous electrodes.<sup>50</sup> A reduction of overall intensity on subsequent cycles indicates a partially reversible characteristic of this reaction. The peak at 0.3–0.9 V can be attributed to the formation of solid electrolyte interphase (SEI) films.<sup>51</sup> From the second to the tenth cycle, there is no clear change, implying that the SEI film and electrode are stable after the first cycle. No peaks of NiO or other impurities are observed, indicating that the graphene is the exclusive active component in the electrode (Figure S12). Figure 5b shows the galvanostatic discharge/charge profiles of DHPG electrodes at a current density of 0.1 A g<sup>-1</sup>. The DHPG electrodes exhibit reversible capacities of 1137 and 957 mAh g<sup>-1</sup> in the first and tenth cycles, respectively, which are  $\sim 3$  times of the theoretical capacity of graphite and also much higher than those of the pristine graphene electrode (577 mAh g<sup>-1</sup> in the first cycle and 429 mAh g<sup>-1</sup> after 10 cycles, Figure S11b). In addition, the Coulombic efficiency in the first cycle increases from 44% for the pristine graphene to 52% for the DHPG.

In the CV and charge/discharge curves, it is observed that redox peaks and potential plateaus are not distinguishable, implying the presence of multiple Li storage positions in DHPG electrodes. It should be noted that the Li storage in DHPG is not an electric double-layer capacitor (EDLC) behavior, and the capacity from lithium ion adsorption on the surface of graphene is negligible due to the relatively low surface area (Figure S13). The capacity of the potential region lower than 0.5 V should be due to lithium intercalation into the graphene layers, while the absence of a potential plateau suggests a disordered stacking of the graphene nanosheet structures, resulting in electrochemically and geometrically non-equivalent Li ion sites.<sup>23,24</sup> The capacity above 0.5 V may be associated with lithium insertion/extraction from the defects in the DHPG electrodes, such as pores, vacancies, and edges of

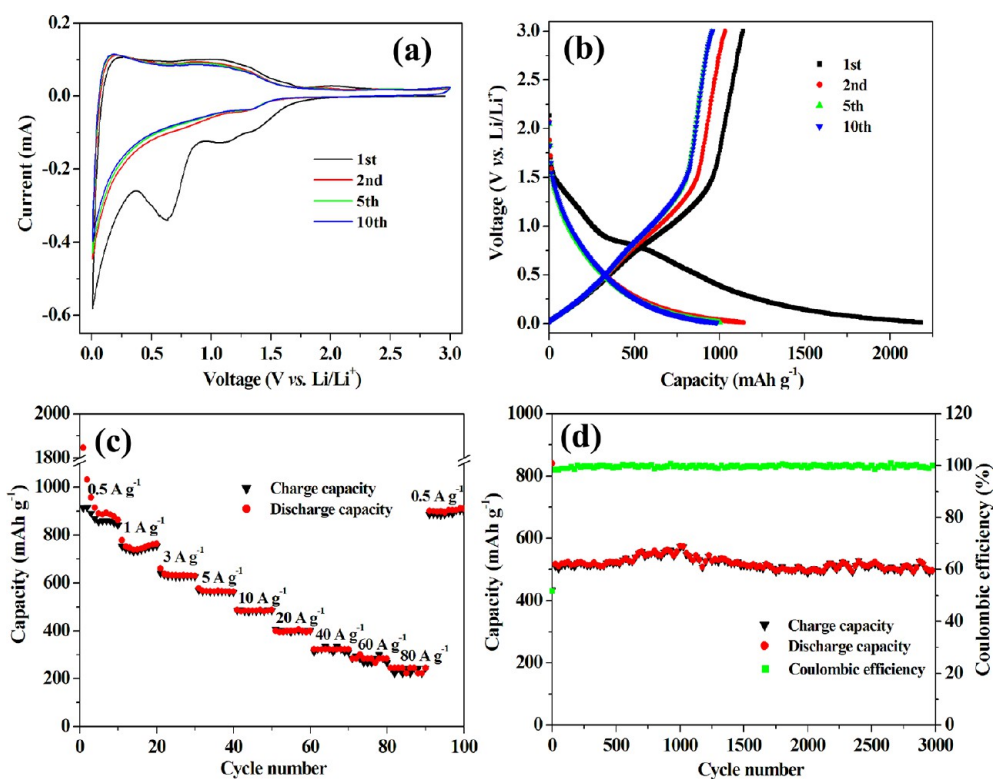


**Figure 5.** Electrochemical performance of DHPG electrodes: (a) cyclic voltammograms at a scan rate of  $0.1 \text{ mV s}^{-1}$ ; (b) charge–discharge curves at  $0.1 \text{ A g}^{-1}$ ; (c) capacity over cycling at different current densities; (d) cycling and Coulombic efficiency at current density of  $5 \text{ A g}^{-1}$ .

the graphene layers.<sup>52,53</sup> Similar Li storage behavior can also be observed in hard carbon. The large irreversible capacity occurring in the first discharge/charge cycle is a common phenomenon for carbon materials due to the formation of SEI films on the electrode surface.<sup>23–32</sup> To increase the initial efficiency, one feasible approach is preforming the SEI layer on the anode materials before use.<sup>54,55</sup> For our DHPG electrodes, the initial Coulombic efficiency can be improved to 94% by simply placing the electrolyte-wetted DHPG electrodes in direct contact with Li foil for about 15–20 min (Figure S14).

Another significant improvement of the DHPG electrode for LIBs is their superior charge and discharge performance. It can be seen that the DHPG electrodes show very high capacity and good stability even at high current densities (Figure 5c). At a current density of  $0.5 \text{ A g}^{-1}$ , the DHPG electrodes can be reversibly charged to  $860 \text{ mAh g}^{-1}$  in about 1.75 h. Furthermore, at a current density of  $5 \text{ A g}^{-1}$  with a charge time of 7 min, the reversible capacities can reach  $560 \text{ mAh g}^{-1}$ . Most significantly, the DHPG electrodes can be fully charged very fast in tens of seconds. At an ultrahigh current density of  $80 \text{ A g}^{-1}$ , corresponding to a charge time of 10 s, the reversible capacities can still reach a high value of  $220 \text{ mAh g}^{-1}$ , showing an ultrahigh rate capability of DHPG electrodes for LIBs (Figure S15a). These results are far more superior to those of the pristine graphene and other carbon materials, such as

graphite, mesoporous carbon, carbon nanotubes, and carbon nanofibers, highlighting the power of the DHPG electrodes as very promising high-rate and large-capacity electrodes for next-generation LIBs.<sup>23–32,50–57</sup> Furthermore, a capacity of  $900 \text{ mAh g}^{-1}$  can be recovered once the current density is restored to the initial  $0.5 \text{ A g}^{-1}$ , implying a very good reversibility. Furthermore, the DHPG electrodes also exhibit long cycling stability at a high current density. As shown in Figure 5d, the cell maintains good capacity retention up to 3000 cycles at a current density of  $5 \text{ A g}^{-1}$ , and even increasing the current density to  $10 \text{ A g}^{-1}$ , the cell can still keep high cycle stability for 2000 cycles with a high capacity of around  $470 \text{ mAh g}^{-1}$  (Figure S15b). It should be noted that the porous graphene assemblies are still anchored on the nickel foam after cycling (Figure S16), demonstrating the high stability of DHPG electrodes.

The most important advantage of the DHPG electrode is simultaneous achievement of supercapacitor-like power density and battery-like energy density. A performance comparison of DHPG and pristine graphene electrodes is highlighted in the Ragone plots in Figure S17a. The specific power density of DHPG electrodes, calculated by integrating the charge curves,<sup>32</sup> is much higher than that of pristine graphene electrodes and comparable to that of supercapacitors while having orders of magnitude larger energy density. At a current density of  $0.5 \text{ A g}^{-1}$ , the DHPG electrodes

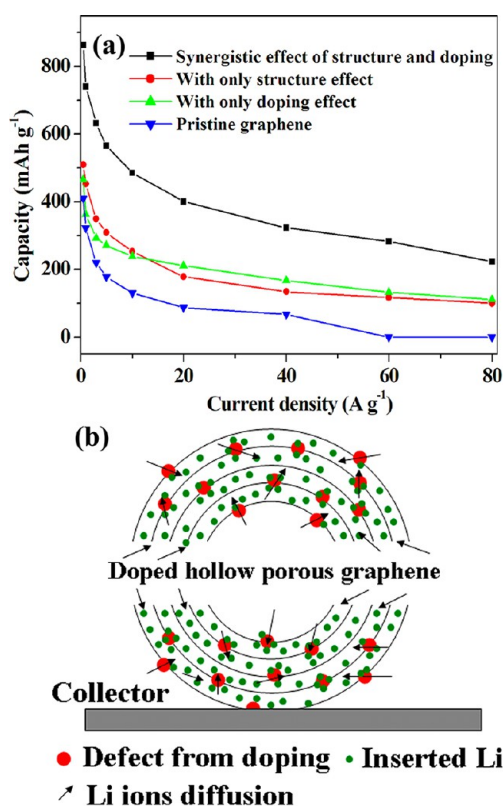


**Figure 6.** (a) Comparison of lithium storage performance with different effect and pristine graphene; (b) Li storage model of *in situ* constructed doped porous multiple-layer graphene in the DHPG electrodes.

deliver a maximum energy density of 867 Wh kg<sup>-1</sup> with a power density of more than 481 W kg<sup>-1</sup>. More surprisingly, at a very high charge/discharge rate in 10 s (80 A g<sup>-1</sup>), the power density reaches 116 kW kg<sup>-1</sup> while the energy density can still maintain 322 Wh kg<sup>-1</sup>, which is much higher than those of the pristine graphene (51 kW kg<sup>-1</sup> and 71 Wh kg<sup>-1</sup> at 40 A g<sup>-1</sup>). To the best of our knowledge, this is the highest level for graphene achieved in LIBs reported to date. The ultrafast charge and discharge capability of DHPG electrodes opens a new avenue to break through the power density limitation of LIBs for high-power applications.

The superior electrochemical performance of the DHPG electrodes can be reasonably attributed to the synergistic effect of the unique electrode structure and heteroatom doping of the graphene. As shown in Figure 6a, the two factors of the structure effect and doping effect are almost equally important, and if without integrative structure or without N,S-doping, the performance is affected greatly (Figures S18 and S19). At 5 A g<sup>-1</sup>, the capacity with both structure and doping effects (560 mAh g<sup>-1</sup>) is much larger than that with only structure effect (309 mAh g<sup>-1</sup>) or doping effect (271 mAh g<sup>-1</sup>). More importantly, compared to the capacity of pristine graphene (178 mAh at 5 A g<sup>-1</sup>), the increase of capacity with both structure and

doping effects (382 mAh g<sup>-1</sup>) is larger than that of the sum with each effect (131 + 93 = 224 mAh g<sup>-1</sup>), that is to say  $E_{\text{structure+doping}} > E_{\text{structure}} + E_{\text{doping}}$ . At all of the current densities, there is the same phenomenon. It is obviously demonstrated that the synergistic effect of structure and doping in the graphene occurs during the electrochemical reactions.

Ionic and electronic transport kinetics lies at the heart of energy storage and conversion systems. An ideal architecture of an electrode for providing efficient ion and electron transport should consist of a 3D interpenetrating network of electron and ion pathways.<sup>38</sup> In our case, the binder-free interconnected porous structure of graphene combined with the macroporous framework of Ni foam provides effective electrolyte transport and Li<sup>+</sup> diffusion and creates a sufficient contact interface between the electrolyte and active materials. Meanwhile, the hollow porous graphene grows together during high-temperature treatment, which alleviates the junction resistance between neighboring sheets. Furthermore, the graphene sphere assemblies *in situ* grow on the skeletons of the Ni foam, providing a direct path for the fast transport of electrons. As shown in Figure S17b, the Nyquist plots reveal that the electrolyte resistance ( $R_{\Omega} = 5.3 \Omega$ ) and charge transfer resistance ( $R_{CT} = 33.5 \Omega$ ) of DHPG electrodes are much lower than those of the pristine graphene electrodes ( $R_{\Omega} = 10.8 \Omega$ ,  $R_{CT} = 56.1 \Omega$ ). In addition, N,S-codoping simultaneously increases the electrical conductivity and electrochemical activity of graphene in the high-rate electrochemical process. The topological defects produced during the doping process may enable the doped graphene to be favorable for Li storage and consequently improve the reversible capacity.<sup>41–45</sup> The Li storage model of DHPG electrodes is suggested in Figure 6b. Some Li ions may be stored reversibly between graphene layers, and a large part of Li ions involve the defect-based reversible storage. The N,S-doping process generates extrinsic defects in the basal plane of graphene, through which Li ions can diffuse into interlayer space of graphene sheets, thus making full use of the interlayer space for Li storage, and also provides more favorable binding of doped sites with Li ions.<sup>45</sup> Moreover, the enlarged *d* spacing could also increase the Li storage performance. Recently, the theoretical calculation method was used to try to explain the phenomenon of lithium storage in graphene layers and emphasize the important roles of defects in the graphene anodes,<sup>41,42</sup> which is consistent with our results. When the special structure effect combines with the heteroatom doping effect, two effects interact and simultaneously improve the performance of lithium storage, which leads to the favorable synergistic effect of the DHPG-based LIB anode.

The working potential of the anode is generally lower than 3.0 V versus Li<sup>+</sup>/Li,<sup>58</sup> and from the aspect

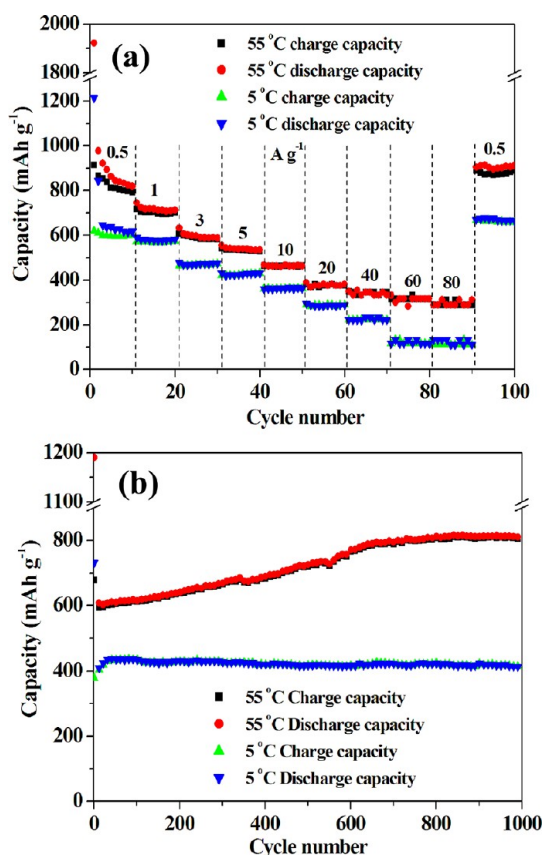


**Figure 7.** (a) Rate capabilities of DHPG electrodes at 5 and 55 °C; (b) cycle performance of DHPG electrodes at 5 A g<sup>-1</sup> at 5 and 55 °C.

of the materials' research, the charge cutoff voltage of the anode materials is usually assigned to 3.0 V, which is widely applied in the carbon-based anode research,<sup>23–30,32,41–45,51–57</sup> and the charge cutoff voltage of 3.0 V may reflect the maximum performance in the half cells. For the convenience of comparable study, we carry out the test with the widely used conditions (0.01–3.0 V). At the same time, considering operating voltage of the full cell, we also carry out the test at the charge cutoff voltage of 1.5 V. As expected, the DHPG electrodes also exhibit excellent performance in the potential range of 0.01–1.5 V (Figure S20). At 1 A g<sup>-1</sup>, the capacity can reach 510 mAh g<sup>-1</sup>, and at 5 A g<sup>-1</sup>, the capacity remains at 380 mAh g<sup>-1</sup> for 2000 cycles with only about 5% loss. Moreover, even at 80 A g<sup>-1</sup>, the capacity could remain at 100 mAh g<sup>-1</sup>. As a common phenomenon for carbon materials, the low charge cutoff voltage would lead to low initial Coulombic efficiency, but this problem can be solved by prelithiation treatment (Figure S12).

As a device that delivers high power, the Joule effect should be considered because large heat can be generated during the charge/discharge process at high power.<sup>59</sup> Meanwhile, the low-temperature performance is also a very important aspect from the

viewpoint of practical applications. Therefore, it is crucial to study the temperature-dependent performance. Measurements are carried out at 55, 5, and –20 °C. Figure 7a clearly shows that, with the increase of temperature, the rate capability significantly improves. Surprisingly, at 80 A g<sup>-1</sup>, the capacity can maintain 280 mAh g<sup>-1</sup>. Furthermore, the DHPG anodes also show excellent cyclability with high capacity at high current density (Figure 7b). The capacity can reach 810 mAh g<sup>-1</sup> even after 1000 cycles at 5 A g<sup>-1</sup>. The increase in capacity with cycling can be attributed to the further activation process of the DHPG anode at high temperature due to the accelerating ion movement. As the temperature increases, the resistance of the cell decreases and the ion mobility in the electrolyte can be enhanced. At low temperature (5 °C), the rate performance slightly decreases due to the low-temperature-induced high resistance but still delivers high capacities. At 0.5 and 80 A g<sup>-1</sup>, the capacities correspond to 610 and 120 mAh g<sup>-1</sup> (Figure 7a), respectively. Importantly, the cell shows excellent cycling stability, and no obvious capacity loss is observed after 1000 cycles at a current density of 5 A g<sup>-1</sup> (Figure 7b). More interestingly, the cell can work at –20 °C and exhibit a high capacity of 220 mAh g<sup>-1</sup> with good cycling at 1 A g<sup>-1</sup> (Figure S21). The high performance of DHPG electrodes over a wide temperature range is a very beneficial feature and expands the range of applications of LIBs.

## CONCLUSIONS

In summary, the synergistic effect of structure and doping in the graphene has been clearly demonstrated for ultrafast and long-cycling rechargeable lithium storage by a facile and effective *in situ* constructing method using freeze-dry technology. It could deliver a high-power density of 116 kW kg<sup>-1</sup>, while the energy density remains as high as 322 Wh kg<sup>-1</sup>, which provides an electrochemical storage level with the power density of a supercapacitor and the energy density of a battery. This is the highest storage level achieved in LIBs for graphene reported to date. Furthermore, the optimized electrodes exhibit long-cycling capability with nearly no capacity loss for 3000 cycles and wide temperature features with high capacities ranging from –20 to 55 °C. Such superior performance of graphene electrodes is attributed to the synergistic effect of the hierarchically porous structure, highly conductive network, and heteroatom doping, which facilitates mass transport and fast electrochemical reactions simultaneously. This study highlights the importance and provides a promising example of rational electrode design and opens up a promising strategy to develop high-performance energy-storage devices. Furthermore, the design

principle and optimized graphene electrode construction can be expanded to other applications including

fuel cells, metal–air cells, and other energy-storage devices.

## EXPERIMENTAL SECTION

**Synthesis of DHPG Electrodes.** GO is synthesized following the literature procedure.<sup>60</sup> Nickel foam (110 PPI, 420 g m<sup>-2</sup>) is first washed with dilute HCl solution and then cut into electrode disks with a diameter of 1.2 cm and a thickness of 1.4 mm. In a typical preparation process, GO (4 mL, 0.5 wt %) solution is dispersed by sonication for 4 h and then PVP surfactant (40 mg) and S-PS spheres (1 g) are added in the GO solution. After stirring and sonication, the colloidal mixture is dropped into the nickel foam disks and then frozen in a refrigerator for 2 h. The water in the resulting gel is removed from the pores of the gel network by a freeze-dry technology. The dry gel embedded in the nickel foam is calcinated in N<sub>2</sub> at 400 °C for 2 h and then at 800 °C for 2 h, and the obtained products are DHPG electrodes that could be directly used as the anode of LIBs. For comparison, the samples with only doping effect are synthesized without nickel foam, and the samples with only structure effect are synthesized without PVP and sulfonated PS. The mass of carbon in the nickel foam is measured by sonication of the DHPG electrode and etching Ni particles with HCl solution. On average, the mass of active material in each electrode is 0.6 mg.

**Material Characterization.** The morphology is observed with scanning electron microscopy (SEM, HITACHI S-4800) operated at 10 kV and transmission electron microscopy (TEM, FEI Tecnai G2) with an accelerating voltage of 200 kV. X-ray photoelectron spectroscopy (XPS) measurements are performed on an ESCA-LAB 250 photoelectron spectrometer. Raman spectra are measured and collected using a 633 nm laser by a Lab RAM HR800. The specific surface areas are determined by a Micromeritics ASAP 2020 analyzer.

**Electrochemical Measurements.** The electrochemical performance of the DHPG electrodes is measured with 2035 coin cells. Lithium foil is used as the anode, 1 mol L<sup>-1</sup> LiPF<sub>6</sub> in a mixture of ethylene carbonate (EC) and dimethyl carbonate (DMC) (1:1, by volume) as electrolyte, and Celgard 2300 as separator. The galvanostatic charge/discharge tests are carried out in the potential of 0.01–3.0 V and 0.01–1.5 V vs Li<sup>+</sup>/Li on a Land CT2001A (China). The capacities of batteries are based on the weight of graphene only. Cyclic voltammetry and electrochemical impedance spectra are measured by a VMP3 electrochemical workstation (Biologic Inc.).

**Conflict of Interest:** The authors declare no competing financial interest.

**Acknowledgment.** The authors greatly appreciated the editor and referees for their constructive comments and insightful suggestions on this manuscript. This work is financially supported by 100 Talents Programme of The Chinese Academy of Sciences, Foundation for Innovative Research Groups of the National Natural Science Foundation of China (Grant No. 20921002) and National Natural Science Foundation of China (Grant No. 21101147 and 21203176).

**Supporting Information Available:** Experimental details, SEM and TEM images, Raman spectrum, atomic force microscopy image, and electrochemical data of samples. This material is available free of charge via the Internet at <http://pubs.acs.org>.

## REFERENCES AND NOTES

- Kang, B.; Ceder, G. Battery Materials for Ultrafast Charging and Discharging. *Nature* **2009**, *458*, 190–193.
- Tarascon, J. M.; Armand, M. Issues and Challenges Facing Rechargeable Lithium Batteries. *Nature* **2001**, *414*, 359–367.
- Chan, C. K.; Peng, H. L.; Liu, G.; McIlwrath, K.; Zhang, X. F.; Huggins, R. A.; Cui, Y. High Performance Lithium Battery Anodes Using Silicon Nanowires. *Nat. Nanotechnol.* **2008**, *3*, 31–35.
- Ji, H. X.; Zhang, L. L.; Pettes, M. T.; Li, H. F.; Chen, S. S.; Shi, L.; Piner, R.; Ruoff, R. S. Ultra-thin Graphite Foam: A Three-Dimensional Conductive Network for Battery Electrodes. *Nano Lett.* **2012**, *12*, 2446–2451.
- Wu, X. L.; Jiang, L. Y.; Cao, F. F.; Guo, Y. G.; Wan, L. J. LiFePO<sub>4</sub> Nanoparticles Embedded in a Nanoporous Carbon Matrix: Superior Cathode Material for Electrochemical Energy-Storage Devices. *Adv. Mater.* **2009**, *21*, 2710–2714.
- Lee, S. W.; Yabuuchi, N.; Gallant, B. M.; Chen, S.; Kim, B. S.; Hammond, P. T.; Shao-Horn, Y. High-Power Lithium Batteries from Functionalized Carbon-Nanotube Electrodes. *Nat. Nanotechnol.* **2010**, *5*, 531–537.
- Hwang, H.; Kim, H.; Cho, J. MoS<sub>2</sub> Nanoplates Consisting of Disordered Grapheme-like Layers for High Rate Lithium Battery Anode Materials. *Nano Lett.* **2011**, *11*, 4826–4830.
- Zhao, L.; Hu, Y. S.; Li, H.; Wang, Z. X.; Chen, L. Q. Porous Li<sub>4</sub>Ti<sub>5</sub>O<sub>12</sub> Coated with N-Doped Carbon from Ionic Liquids for Li-Ion Batteries. *Adv. Mater.* **2011**, *23*, 1385–1388.
- Simon, P.; Gogotsi, Y. Materials for Electrochemical Capacitors. *Nat. Mater.* **2008**, *7*, 845–854.
- Wu, Q.; Xu, Y. X.; Yao, Z. Y.; Liu, A. R.; Shi, G. Q. Supercapacitors Based on Flexible Graphene/Polyaniline Nanofiber Composite Films. *ACS Nano* **2010**, *4*, 1993–1970.
- Wang, B.; Chen, J. S.; Wu, H. B.; Wang, Z.; Lou, X. W. Quasiemulsion-Templated Formation of α-Fe<sub>2</sub>O<sub>3</sub> Hollow Spheres with Enhanced Lithium Storage Properties. *J. Am. Chem. Soc.* **2011**, *133*, 17146–17148.
- Jung, H. G.; Jang, M. W.; Hassoun, J.; Sun, Y. K.; Scrosati, B. A High-Rate Long-Life Li<sub>4</sub>Ti<sub>5</sub>O<sub>12</sub>/Li[Ni<sub>0.45</sub>Co<sub>0.1</sub>Mn<sub>1.45</sub>]O<sub>4</sub> Lithium-Ion Battery. *Nat. Commun.* **2011**, *2*, 516.
- Cheng, F. Y.; Liang, J.; Tao, Z. L.; Chen, J. Functional Materials for Rechargeable Batteries. *Adv. Mater.* **2011**, *23*, 1695–1715.
- Wang, Y. G.; Wang, Y. R.; Hosono, E.; Wang, K. X.; Zhou, H. S. The Design of a LiFePO<sub>4</sub>/Carbon Nanocomposite with a Core–Shell Structure and Its Synthesis by an *In Situ* Polymerization Restriction Method. *Angew. Chem., Int. Ed.* **2008**, *47*, 7461–7465.
- Novoselov, K. S.; Geim, A. K.; Morozov, S. V.; Jiang, D.; Zhang, Y.; Dubonos, S. V.; Grigorieva, I. V.; Firsov, A. A. Electric Field Effect in Atomically Thin Carbon Films. *Science* **2004**, *306*, 666–669.
- Geim, A. K.; Novoselov, K. S. The Rise of Graphene. *Nat. Mater.* **2007**, *6*, 183–191.
- Song, Z. P.; Xu, T.; Gordin, M. L.; Jiang, Y. B.; Bae, I. T.; Xiao, Q. F.; Zhan, H.; Liu, J.; Wang, D. H. Polymer–Graphene Nanocomposites as Ultrafast-Charge and -Discharge Cathodes for Rechargeable Lithium Batteries. *Nano Lett.* **2012**, *12*, 2205–2211.
- Huang, X.; Qi, X. Y.; Boey, F.; Zhang, H. Graphene-Based Composites. *Chem. Soc. Rev.* **2012**, *41*, 666–686.
- Zhu, Y.; Murali, S.; Cai, W.; Li, X.; Suk, J. W.; Potts, J. R.; Ruoff, R. S. Graphene and Graphene Oxide: Synthesis, Properties, and Applications. *Adv. Mater.* **2010**, *22*, 3906–3924.
- Liang, M.; Zhi, L. Graphene-Based Electrode Materials for Rechargeable Lithium Batteries. *J. Mater. Chem.* **2009**, *19*, 5871–5878.
- Wu, Z. S.; Yang, S. B.; Sun, Y.; Parvez, K.; Feng, X. L.; Müllen, K. 3D Nitrogen-Doped Graphene Aerogel-Supported Fe<sub>3</sub>O<sub>4</sub> Nanoparticles as Efficient Electrocatalysts for the Oxygen Reduction Reaction. *J. Am. Chem. Soc.* **2012**, *134*, 9082–9085.
- Wu, D. Q.; Zhang, F.; Liang, H. W.; Feng, X. L. Nanocomposites and Macroscopic Materials: Assembly of Chemically Modified Graphene Sheets. *Chem. Soc. Rev.* **2012**, *41*, 6160–6177.
- Yoo, E.; Kim, J.; Hosono, E.; Zhou, H.; Kudo, T.; Honma, I. Large Reversible Li Storage of Graphene Nanosheet Families for Use in Rechargeable Lithium Ion Batteries. *Nano Lett.* **2008**, *8*, 2277–2282.

24. Pan, D. Y.; Wang, S.; Zhao, B.; Wu, M. H.; Zhang, H. J.; Wang, Y.; Jiao, Z. Li Storage Properties of Disordered Graphene Nanosheets. *Chem. Mater.* **2009**, *21*, 3136–3142.
25. Guo, P.; Song, H.; Chen, X. Electrochemical Performance of Graphene Nanosheets as Anode Material for Lithium-Ion Batteries. *Electrochem. Commun.* **2009**, *11*, 1320–1324.
26. Bhardwaj, T.; Antic, A.; Pavan, B.; Barone, V.; Fahlman, B. D. Enhanced Electrochemical Lithium Storage by Graphene Nanoribbons. *J. Am. Chem. Soc.* **2010**, *132*, 12556–12558.
27. Lian, P.; Zhu, X.; Liang, S.; Li, Z.; Yang, W.; Wang, H. Large Reversible Capacity of High Quality Graphene Sheets as an Anode Material for Lithium-Ion Batteries. *Electrochim. Acta* **2010**, *55*, 3909–3914.
28. Yang, S. B.; Feng, X. L.; Zhi, L. J.; Cao, Q. A.; Maier, J.; Müllen, K. Nanographene-Constructed Hollow Carbon Spheres and Their Favorable Electroactivity with Respect to Lithium Storage. *Adv. Mater.* **2010**, *22*, 838–842.
29. Yin, S.; Zhang, Y.; Kong, J.; Zou, C.; Li, C. M.; Lu, X.; Ma, J.; Boey, F. Y. C.; Chen, X. Assembly of Graphene Sheets into Hierarchical Structures for High-Performance Energy Storage. *ACS Nano* **2011**, *5*, 3831–3838.
30. Wallace, G. G.; Wang, C. Y.; Li, D.; Too, C. O. Electrochemical Properties of Graphene Paper Electrodes Used in Lithium Batteries. *Chem. Mater.* **2009**, *21*, 2604–2606.
31. Zhao, X.; Hayner, C. M.; Kung, M. C.; Kung, H. H. Flexible Holey Graphene Paper Electrodes with Enhanced Rate Capability for Energy Storage Applications. *ACS Nano* **2011**, *5*, 8739–8749.
32. Wu, Z. S.; Ren, W. C.; Xu, L.; Li, F.; Cheng, H. M. Doped Graphene Sheets as Anode Materials with Superhigh Rate and Large Capacity for Lithium Ion Batteries. *ACS Nano* **2011**, *5*, 5463–5471.
33. Jang, B. Z.; Liu, C. G.; Neff, D.; Yu, Z. N.; Wang, M. C.; Xiong, W.; Zhamu, A. Graphene Surface-Enabled Lithium Ion-Exchanging Cells: Next-Generation High-Power Energy Storage Devices. *Nano Lett.* **2011**, *11*, 3785–3791.
34. Yao, Y.; McDowell, T. M.; Ryu, I.; Wu, H.; Liu, N.; Hu, L. B.; Nix, W. D.; Cui, Y. Interconnected Silicon Hollow Nanospheres for Lithium-Ion Battery Anodes with Long Cycle Life. *Nano Lett.* **2011**, *11*, 2949–2954.
35. Xu, Y. X.; Sheng, K. X.; Li, C.; Shi, G. Q. Self-Assembled Graphene Hydrogel via a One-Step Hydrothermal Process. *ACS Nano* **2010**, *4*, 4324–4330.
36. Sun, Y. M.; Hu, X. L.; Yu, J. C.; Li, Q.; Luo, W.; Yuan, L. X.; Zhang, W. X.; Huang, Y. H. Morphosynthesis of Hierarchical MoO<sub>2</sub> Nanoarchitectures as a Binder-Free Anode for Lithium-Ion Batteries. *Energy Environ. Sci.* **2011**, *4*, 2870–2877.
37. Choi, B. G.; Yang, M. H.; Hong, W. H.; Choi, J. W.; Huh, Y. S. 3D Macroporous Graphene Frameworks for Supercapacitors with High Energy and Power Densities. *ACS Nano* **2012**, *6*, 4020–4028.
38. Zhang, H. G.; Yu, X. D.; Braun, P. V. Three-Dimensional Bicontinuous Ultrafast-Charge and Discharge Bulk Battery Electrodes. *Nat. Nanotechnol.* **2011**, *6*, 277–281.
39. Wu, Z. S.; Winter, A.; Chen, L.; Sun, Y.; Turchanin, A.; Feng, X. L.; Müllen, K. Three-Dimensional Nitrogen and Boron Codoped Graphene for High-Performance All-Solid-State Supercapacitors. *Adv. Mater.* **2012**, *24*, 5130–5135.
40. Su, Y. Z.; Li, S.; Wu, D. Q.; Zhang, F.; Liang, H. W.; Gao, P. F.; Cheng, C.; Feng, X. L. Two-Dimensional Carbon-Coated Graphene/Metal Oxide Hybrids for Enhanced Lithium Storage. *ACS Nano* **2012**, *6*, 8349–8356.
41. Yao, F.; Gunes, F.; Ta, H. Q.; Lee, S. M.; Chae, S. J.; Sheem, K. Y.; Cojocaru, C. S.; Xie, S. S.; Lee, Y. H. Diffusion Mechanism of Lithium Ion through Basal Plane of Layered Graphene. *J. Am. Chem. Soc.* **2012**, *134*, 8646–8654.
42. Lee, E.; Persson, K. A. Li Absorption and Intercalation in Single Layer Graphene and Few Layer Graphene by First Principles. *Nano Lett.* **2012**, *12*, 4624–4628.
43. Reddy, A. L. M.; Srivastava, A.; Gowda, S. R.; Gullapalli, H.; Dubey, M.; Ajayan, P. M. Synthesis of Nitrogen-Doped Graphene Films for Lithium Battery Application. *ACS Nano* **2010**, *4*, 6337–6342.
44. Jeong, H. M.; Lee, J. W.; Shin, W. H.; Choi, Y. J.; Shin, H. J.; Kang, J. K.; Choi, J. W. Nitrogen-Doped Graphene for High-Performance Ultracapacitors and the Importance of Nitrogen-Doped Sites at Basal Planes. *Nano Lett.* **2011**, *11*, 2472–2477.
45. Shin, W. H.; Jeong, H. M.; Kim, B. G.; Kang, J. K.; Choi, J. W. Nitrogen-Doped Multiwall Carbon Nanotubes for Lithium Storage with Extremely High Capacity. *Nano Lett.* **2012**, *12*, 2283–2288.
46. Wohlgemuth, S. A.; White, R. J.; Willinger, M. G.; Titirici, M. M.; Antonietti, M. A One-Pot Hydrothermal Synthesis of Sulfur and Nitrogen Doped Carbon Aerogels with Enhanced Electrocatalytic Activity in the Oxygen Reduction Reaction. *Green Chem.* **2012**, *14*, 1515–1523.
47. Yang, Z.; Yao, Z.; Li, G. F.; Fang, G. Y.; Nie, H. G.; Liu, Z.; Zhou, X. M.; Chen, X. A.; Huang, S. M. Sulfur-Doped Graphene as an Efficient Metal-Free Cathode Catalyst for Oxygen Reduction. *ACS Nano* **2012**, *6*, 205–211.
48. Sheng, Z. H.; Tao, L.; Chen, J. J.; Bao, W. J.; Wang, F. B.; Xia, X. H. Catalyst-Free Synthesis of Nitrogen-Doped Graphene via Thermal Annealing Graphite Oxide with Melamine and Its Excellent Electrocatalysis. *ACS Nano* **2011**, *5*, 4350–4358.
49. Li, X. L.; Wang, H. L.; Robinson, J. T.; Sanchez, H.; Diankov, G.; Dai, H. J. Simultaneous Nitrogen Doping and Reduction of Graphene Oxide. *J. Am. Chem. Soc.* **2009**, *131*, 15939–15944.
50. Matsumura, Y.; Wang, S.; Mondori, J. Mechanism Leading to Irreversible Capacity Loss in Li Ion Rechargeable Batteries. *J. Electrochem. Soc.* **1995**, *142*, 2914–2918.
51. Tang, K.; White, R. J.; Mu, X.; Titirici, M. M.; Aken, P. V.; Maier, J. Hollow Carbon Nanospheres with a High Rate Capability for Lithium-Based Batteries. *ChemSusChem* **2012**, *5*, 400–403.
52. Mao, Y.; Duan, H.; Xu, B.; Zhang, L.; Hu, Y. S.; Zhao, C. C.; Wang, Z. X.; Chen, L. Q.; Yang, Y. S. Lithium Storage in Nitrogen-Rich Mesoporous Carbon Materials. *Energy Environ. Sci.* **2012**, *5*, 7950–7955.
53. Han, F. D.; Bai, Y. J.; Liu, R.; Yao, B.; Qi, Y. X.; Lun, N.; Zhang, J. X. Template-Free Synthesis of Interconnected Hollow Carbon Nanospheres for High-Performance Anode Material in Lithium-Ion Batteries. *Adv. Energy Mater.* **2011**, *1*, 798–801.
54. Hassoun, J.; Lee, K. S.; Sun, Y. K.; Scrosati, B. An Advanced Lithium Ion Battery Based on High Performance Electrode Materials. *J. Am. Chem. Soc.* **2011**, *133*, 3139–3143.
55. Kaskhedikar, N. A.; Maier, J. Lithium Storage in Carbon Nanostructures. *Adv. Mater.* **2009**, *21*, 2664–2680.
56. Hu, Y. S.; Adelhelm, P.; Smarsly, B. M.; Hore, S.; Antonietti, M.; Maier, J. Synthesis of Hierarchically Porous Carbon Monoliths with Highly Ordered Microstructure and Their Application in Rechargeable Lithium Batteries with High-Rate Capability. *Adv. Funct. Mater.* **2007**, *17*, 1873–1878.
57. Xu, Y. J.; Liu, X.; Cui, G. L.; Zhu, B.; Weinberg, G.; Schlogl, R.; Maier, J.; Su, D. S. A Comparative Study on the Lithium-Ion Storage Performances of Carbon Nanotubes and Tube-in-Tube Carbon Nanotubes. *ChemSusChem* **2010**, *3*, 343–349.
58. Choi, N. S.; Chen, Z. H.; Freunberger, S. A.; Ji, X. L.; Sun, Y. K.; Amine, K.; Yushin, G.; Nazar, L. F.; Cho, J.; Bruce, P. G. Challenges Facing Lithium Batteries and Electrical Double-Layer Capacitors. *Angew. Chem., Int. Ed.* **2012**, *51*, 9994–10024.
59. Zaghbi, K.; Goodenough, J. B.; Mauger, A.; Julien, C. Unsupported Claims of Ultrafast Charging of LiFePO<sub>4</sub> Li-Ion Batteries. *J. Power Sources* **2009**, *194*, 1021–1023.
60. Marcano, D. C.; Kosynkin, D. V.; Berlin, J. M.; Sinitskii, A.; Sun, Z. Z.; Slesarev, A.; Alemany, L. B.; Lu, W.; Tour, J. M. Improved Synthesis of Graphene Oxide. *ACS Nano* **2010**, *4*, 4806–4814.